Soft Matter

Tethered tracer in a mixture of hot and cold Brownian particles: can activity pacify fluctuations?

Journal:	*Soft Matter*
Manuscript ID	SM-ART-08-2021-001163.R1
Article Type:	Paper
Date Submitted by the Author:	24-Sep-2021
Complete List of Authors:	Wang, Michael; New York University, Physics; University of Massachusetts Amherst, Polymer Science and Engineering Zinga, Ketsia; New York University, Physics; The University of Texas at Austin Cockrell School of Engineering, Biomedical Engineering Zidovska, Alexandra; New York University, Department of Physics Grosberg, Alexander; New York University, Physics

Journal Name

ARTICLE TYPE

Cite this: DOI: 00.0000/xxxxxxxxxx

Tethered tracer in a mixture of hot and cold Brownian particles: can activity pacify fluctuations?

Michael Wang[a,b], Ketsia Zinga[a,c], Alexandra Zidovska[a], Alexander Y. Grosberg*[a]

Received Date
Accepted Date

DOI: 00.0000/xxxxxxxxxx

We study how an interacting mixture of components with differing levels of activity can affect the fluctuations of an embedded object such as a tracer. In particular, we consider a simple model of a tracer that is harmonically bound within a mixture of hot and cold Brownian particles, which, like a mixture of active and passive particles, can phase separate. By measuring the fluctuations of the tracer, we find that this collective behavior gives rise to an effective temperature for the tracer. Additionally, we find that there is an increased tendency for cold particles to accumulate on the surface of the tracer due to the hot particles, potentially dampening its fluctuations and decreasing its effective temperature. These results suggest that the phase separation of a mixture of hot/cold or active/passive particles may have strong effects on the fluctuations of an embedded object. We discuss potential implications of these results for experiments on fluctuations of nuclear envelope affected by the activity in the chromatin.

1 Introduction

Active systems, driven by consuming and dissipating energy from some source, such as ATP hydrolysis in biological systems, or other chemical reactions and/or light in experimental systems, usually exhibit some non-thermal fluctuations in addition to the regular thermal ones. For thermal fluctuations close to equilibrium, the familiar fluctuation dissipation theorem holds (see, e.g., [1]) which states that

$$\left(x^2\right)_\omega = \frac{2k_\mathrm{B}T}{\omega}\chi''_\omega\,, \tag{1a}$$

where $\left(x^2\right)_\omega$ is the fluctuation power spectrum of the quantity x at frequency ω, $k_\mathrm{B}T$ is the thermal energy, and χ''_ω is the imaginary part of the appropriate causal response function. In particular, the mean squared value of x averaged over time comes out proportional to the temperature and dependent on the effective spring constant (which, according to Kramers-Kronig relation is the inverse of the real part of the response function at zero frequency):

$$\left\langle x^2\right\rangle = \frac{k_\mathrm{B}T}{K_\mathrm{eff}}\,,\quad \text{with } \frac{1}{K_\mathrm{eff}} = \int_{-\infty}^{\infty}\frac{\chi''_\omega}{\omega}\frac{d\omega}{\pi} = \chi'_\omega|_{\omega=0}\,. \tag{1b}$$

The often followed temptation for driven active systems is to imagine that equations (1) are still valid, albeit with an effective and perhaps frequency-dependent "temperature". This is indeed tempting, because formulas (1) nicely support physical intuition that power of fluctuations must be increasing with intensity of the driving source. For thermal fluctuations, this source is $k_\mathrm{B}T$, while for non-thermal it is something else, but the expectation is that more intense activity should lead to increased fluctuations.

Indeed, this is exactly what is observed in many experiments. For example, the flickering of the red blood cells is stronger at low frequencies than what can be caused by thermal fluctuations alone, indicative of active biological processes in these cells[2]. Similarly, the velocity fluctuations in chromatin are stronger than those due to thermal fluctuations at small wavenumbers, again due to activity. These fluctuations are reduced to purely thermal levels if active processes are artificially inhibited[3,4].

It is against the background of these ideas that we were so surprised by recent experiments examining how the fluctuations of the nuclear envelope are affected by the active processes both inside and outside the cell nucleus[5]. It was found that the cytoskeletal activity, for example of microtubules and myosins, enhances the nuclear shape fluctuations from the outside of the nucleus, while the genome-related activity inside the nucleus dampens those fluctuations. Reducing the cytoskeletal activity led to decrease of these fluctuations, whereas reducing the genome-related activity increased them. Put another way, increasing the motor activity within the genome inside the nucleus can counterintuitively suppress the fluctuations of the nuclear envelope. How can activity reduce fluctuations? We hypothesize that one possible source of this dampening is the active phase separation of chromatin into regions of passive heterochromatin and active

[a] Department of Physics and Center for Soft Matter Research, New York University, 726 Broadway, New York, NY 10003 USA. E-mail: ayg1@nyu.edu
[b] Present address: Department of Polymer Science and Engineering, University of Massachusetts, Amherst, MA 01003 USA
[c] Present address: Department of Biomedical Engineering, University of Texas at Austin, Austin, TX 78712 USA

euchromatin, and in particular, the tendency for heterochromatin to accumulate on surfaces such as the nuclear envelope or nucleoli[6–10].

To address this idea in the simplest setting imaginable, we ask here how a mixture of components with differing levels of activity may affect the behavior of an embedded object such as a membrane or tracer. Specifically, we present here a simple model of a large tracer that is harmonic trapped in a suspension of hot and cold Brownian particles. These hot and cold particles are similar to active and passive particles in that hot particles diffused more rapidly than cold ones just like how active particles propel more strongly than passive ones. Both types of systems exhibit phase separation into regions of hot/active and cold/passive particles[11–15]. This model of hot and cold Brownian particles can often give us useful insights through both analytical theory and simulations (see[16–31]) and is thus a useful model for our present purposes. It should be noted that in many models of active systems, such as active Brownian particles or run-and-tumble particles, an important feature is some level of directional persistence of their motion. Our system of hot and cold particles lacks that. But really the defining property of an active system should be that it has a source of energy that is input to the system on a local scale. We therefore employ the hot-and-cold model to explore the possibility that locally inserted energy may lead to dampening rather than enhancing of fluctuations.

In particular, to characterize the fluctuations of the tracer, we focus on its mean-squared displacement (MSD) $\langle \mathbf{R}^2 \rangle$, from which we can extract the effective temperature $k_B T_{\text{eff}}$ of the tracer due to its interactions with the surrounding suspension of hot and cold particles. This effective temperature tells us how the cooperative effects such as phase separation influence the behavior of the tracer.

2 The model

The model that we study is sketched in Figure 1. It consists of a tracer that is harmonically attached to an immobile pivot and submerged within a suspension composed of N_h hot particles and N_c cold particles. Suppose the tracer is driven by a thermostat with temperature T_{tr} while the hot and cold particles are driven by thermostats with temperatures T_h and T_c, respectively. The overdamped Langevin equations describing this system are

$$0 = -\Gamma \dot{\mathbf{R}} - K\mathbf{R} - \nabla_{\mathbf{R}} U(\mathbf{R}, \{\mathbf{r}_{h,i}\}, \{\mathbf{r}_{c,i}\}) + \sqrt{2k_B T_{tr} \Gamma}\, \xi_{tr}(t) \ , \quad \text{(2a)}$$

$$0 = -\gamma \dot{\mathbf{r}}_{h,i} - \nabla_{\mathbf{r}_{h,i}} U(\mathbf{R}, \{\mathbf{r}_{h,i}\}, \{\mathbf{r}_{c,i}\}) + \sqrt{2k_B T_h \gamma}\, \xi_{h,i}(t) \ , \quad \text{(2b)}$$

$$0 = -\gamma \dot{\mathbf{r}}_{c,i} - \nabla_{\mathbf{r}_{c,i}} U(\mathbf{R}, \{\mathbf{r}_{h,i}\}, \{\mathbf{r}_{c,i}\}) + \sqrt{2k_B T_c \gamma}\, \xi_{c,i}(t) \ , \quad \text{(2c)}$$

where $U(\mathbf{R}, \{\mathbf{r}_{h,i}\}, \{\mathbf{r}_{c,i}\})$ is the total potential energy of the system which is assumed to be pairwise additive, and includes purely repulsive central potentials $U_{tr,h}(|\mathbf{R} - \mathbf{r}_{h,i}|)$ and $U_{tr,c}(|\mathbf{R} - \mathbf{r}_{c,i}|)$ for the interactions between the tracer and the hot/cold particles (with indices standing for the tracer tr, hot h, and cold c), as well as the potentials $U_{h,h}(|\mathbf{r}_{h,i} - \mathbf{r}_{h,j}|)$, $U_{c,c}(|\mathbf{r}_{c,i} - \mathbf{r}_{c,j}|)$, and $U_{h,c}(|\mathbf{r}_{h,i} - \mathbf{r}_{c,j}|)$ for the interactions between the hot and cold particles themselves. K is the stiffness of the harmonic trap or spring that tethers the tracer. Γ and γ are the friction coefficients of the tracer and hot/cold particles, respectively.

We are interested in the fluctuations of the tracer which we characterize by determining its MSD $\langle \mathbf{R}^2 \rangle$. In whatever space dimension d, the Cartesian components of vector $\mathbf{R}$ are statistically independent (because trap is harmonic), and so we measure MSD in only one of the spatial directions, say x. Thus, we determine $\langle x^2 \rangle$, from which we can extract the effective temperature T_{eff} of the tracer through the relation

$$\langle x^2 \rangle = \frac{k_B T_{\text{eff}}}{K} \ , \ \langle \mathbf{R}^2 \rangle = \langle x^2 \rangle d \ . \quad (3)$$

We use this effective temperature to characterize the fluctuations. In other words, we can think of the tracer as a thermometer inserted into a non-equilibrium mixture of hot and cold particles.

This system is difficult to address analytically for an arbitrary potential $U(\mathbf{R}, \{\mathbf{r}_{h,i}\}, \{\mathbf{r}_{c,i}\})$, and so we will resort to the use of Brownian Dynamics simulations, the details of which we relegate to the Appendix section B. Only when the interaction potentials are all harmonic does our system allow for an analytic solution which we present in Appendix section C.

There is one obvious case when we know the answer in advance: if the temperatures are all equal, that is, $T_{tr} = T_h = T_c = T$. In this case, the system is in equilibrium and we know what we should get. By the equipartition theorem, we should have exactly equations (3) with $T_{\text{eff}} = T$. We can go even further to say that positions of the tracer should follow the Boltzmann distribution given by

$$\rho(\mathbf{R}) \propto \exp\left(-\frac{K\mathbf{R}^2}{2k_B T}\right) \ . \quad (4)$$

Note that this equilibrium limit is independent of the surrounding particles and will be extremely useful for thinking about the simulation results later.

In what follows we report the results of Brownian Dynamics simulations based on the Langevin equations (2). In each run, we measure the position vector $\mathbf{R}(t)$ of the tracer as a function of time, square-averaging it over several runs. Two representative examples of the resulting $\langle \mathbf{R}^2 \rangle(t)$ traces are shown in Figure 2. As expected, $\mathbf{R}^2(t)$ in steady state fluctuates around some average value $\langle \mathbf{R}^2 \rangle$, which serves as a measure of the effective temperature according to the equation (3). As regards to the distribution of $\mathbf{R}^2(t)$ around its mean, we do not have general statement for a nonequilibrium system with different temperatures that it should follow a Gaussian distribution. However, we check this distribution numerically and find that in most cases, to within numerical errors, it is pretty close to Gaussian. We will use this distribution to assess the quality of using a tracer as a thermometer. Furthermore, we will test if T_{eff} determined from the average value of $\langle \mathbf{R}^2 \rangle$ using equation (3) is consistent with T_{eff} determined from the width of the distribution.

3 Hot tracer in a cold bath

We start with the case when all of the particles except the tracer are cold and look at how the effective temperature depends on the temperature and density of the surrounding cold particles. We assume that the tracer is in contact with a thermostat at tempera-

ture $T_{\rm Tr} = T_{\rm h} \geq T_{\rm c}$. The tracer interacts with nearby cold particles through a purely repulsive potential (see Appendix section B for details of the model). As regards to the interactions between cold particles, we consider two cases–when cold particles repel one another through a short range excluded volume type potential, and when they do not interact at all.

Figure 3 shows the dependence of the effective temperature of the tracer, determined from the amplitude of fluctuations using formula (3), on the temperature of the cold particles, at a particular area fraction $\phi = 0.4$ (a note of caution: area fraction is conveniently defined for interacting particles having an excluded volume (area); for non-interacting particles we mean the same number density that corresponds to $\phi = 0.4$ for interacting ones). We can make sense of this dependence by considering two limits.

First, consider the case when $T_{\rm c}$ is very low. Let us start with $T_{\rm c} = 0$. In this case, cold particles do not undergo any Brownian motion at all. When the moving tracer pushes them away, they do not come back. As a result, the tracer over time builds around itself a cold-particles-free zone as big as allowed by its harmonic tether. Within this zone, the tracer's fluctuations are governed by its own thermostat, and we therefore should expect $T_{\rm eff} = T_{\rm h}$, in agreement with observations. If $T_{\rm c}$ is not quite 0 but small, the cold particles slowly diffuse back into the void. Consequently, the void becomes somewhat smaller, and so does $T_{\rm eff}$.

In the second limit, when $T_{\rm c}$ is only moderately lower than $T_{\rm h}$, we can think of the situation in the following way. Normally, the Langevin equation describes the motion of a particle, such as our tracer, as a result of two forces, friction and random molecular kicks. Our tracer can be thought of as moving through two fluids simultaneously. One is the regular molecular solvent, already present in the equation (2a), and the other is the liquid of cold particles. The forces exerted by those cold particles on the tracer are written down explicitly in the equation (2a), but we can recast them phenomenologically by saying that all cold particles together conspire to provide an effective friction force $-\Gamma_{\rm c}\dot{\mathbf{R}}$ and random kicks $\sqrt{2\Gamma_{\rm c}T_{\rm c}}\xi_{\rm eff}(t)$. Here we introduced the friction coefficient $\Gamma_{\rm c}$ due to the cold particles, which is the same in both terms, because the cold particles themselves obey the fluctuation-dissipation relation. The resulting effective Langevin equation for the tracer reads

$$0 = -\Gamma\dot{\mathbf{R}} - \Gamma_{\rm c}\dot{\mathbf{R}} - K\mathbf{R} + \sqrt{2k_{\rm B}T_{\rm tr}\Gamma}\xi_{\rm tr}(t) + \sqrt{2\Gamma_{\rm c}T_{\rm c}}\xi_{\rm eff}(t)\ , \quad (5a)$$

It is worth emphasizing that the above equation is phenomenological in nature, and we do not offer any systematic procedure to derive it from first principles. Accordingly, we view the coefficient $\Gamma_{\rm c}$ as a phenomenological parameter to be determined from simulations. Physically, we expect this equation to be applicable when tracer particle is significantly larger in size than cold particles. Since the noises $\xi_{\rm tr}(t)$ and $\xi_{\rm eff}(t)$ are statistically independent, the last two terms can be combined to yield

$$0 = -(\Gamma+\Gamma_{\rm c})\dot{\mathbf{R}} - K\mathbf{R} + \sqrt{2k_{\rm B}T_{\rm h}\Gamma + 2k_{\rm B}T_{\rm c}\Gamma_{\rm c}}\xi(t)\ . \quad (5b)$$

This looks exactly like a regular Langevin equation for a single particle in a harmonic trap $K\mathbf{R}^2/2$ with a friction coefficient $\Gamma+\Gamma_{\rm c}$ and an effective temperature

$$T_{\rm eff} = \frac{T_{\rm h}\Gamma + T_{\rm c}\Gamma_{\rm c}}{\Gamma+\Gamma_{\rm c}}\ . \quad (6)$$

A similar expression for the effective temperature's linearly dependence on $T_{\rm c}$ is also found by a more explicit but model-dependent calculation in the Appendix section C (see formula (12)). There, we assumed that all the particles interact with the tracer via harmonic springs and expressed $\Gamma_{\rm c}$ in terms of the spring constants and numbers of connected cold particles. Thus, one way or another, we expect the effective temperature to be a linear function of $T_{\rm c}$, consistent with our numerical observations. Figure 3 shows also that the slope, obviously controlled by the phenomenological parameter $\Gamma_{\rm c}$, is somewhat different for interacting and non-interacting cold particles; it makes intuitive sense that this quantity is somewhat smaller for the non-interacting cold particles.

Next we examine the distribution of $\mathbf{R}^2$ at various values of $T_{\rm c}$, and find that it is indistinguishable from the Gaussian within the accuracy of our simulations, as shown in Figure 4 for interacting cold particles and in the Appendix Figure 12 for non-interacting ones. This accurate collapse of the distributions onto a single Gaussian master curve at several values of $T_{\rm c}$ supports the ansatz leading to formula (6).

Figure 5, left panel, shows the effective temperature and its dependence on the packing fraction of the cold suspension. Not surprisingly, the effective temperature decreases as the density of cold particles increases. As the number of cold particles surrounding the tracer increases, more and more of the tracer's energy is transferred to the cold particles through work. To gain a better insight, we resort again to equation (6); there, the dependence on cold particles density must be hidden in the friction coefficient $\Gamma_{\rm c} = \Gamma_{\rm c}(\phi)$. We solve equation (6) for $\Gamma_{\rm c}$ and use the data of Figure 5 left panel to obtain $\Gamma_{\rm c}(\phi)$; it is plotted in the right panel in Figure 5. Not surprisingly, the friction coefficient increases with increasing density. For non-interacting cold particles, the dependence on the density is linear, which is very natural, as every particle acts independently of others; the fitted slope, $\Gamma_{\rm c}/\Gamma \approx 2.8\phi$, looks superficially similar to Einstein's prediction of 2.5ϕ [32,33]; this closeness is, however, just fortuitous, because our system is 2D and our particles experience friction against an immobile background, while Einstein's is due to real hydrodynamics in 3D. For interacting cold particles, the friction is the same in the very dilute limit, but then grows faster with density, leading to the larger tracer friction coefficient. In that case, the dependence $\Gamma_{\rm c}(\phi)$ fits rather well to the expression $\Gamma_{\rm c}/\Gamma \approx 2.8\phi + 33.9\phi^3$, as shown by the line in the figure. Intriguingly, this cubic function of density fits better than a quadratic one; why it is cubic is not entirely clear to us. One possibility is related to the fact that suspensions of spherical particles often exhibit strong shear thickening behavior (see, e.g., [34]) which might be relevant in our case given the significant difference between temperatures.

In Figure 6 for interacting cold particles (and in the Appendix Figure 13 for noninteracting ones) we check again that the distribution of $\mathbf{R}^2$ remains Gaussian at all densities tested, and has a width consistent with effective temperature obtained in Figure 5.

4 Tracer particle in a mixed bath of cold and hot particles

We now turn our attention to a mixture of hot and cold particles. The interactions between the hot and cold particles are responsible for the possible activity-based phase separation, as shown pictorially in Figure 7. There, we show representative snapshots of the system at several values of the global fraction of hot particles, defined as $f_h = N_h/(N_h+N_c)$, where N_h and N_c are the global numbers of hot and cold particles, respectively. As expected, phase separation is observed at for intermediate values of f_h.

To get a sense of how interactions within the surrounding mixture of hot and cold particles affect the tracer, we consider two cases when the surrounding mixture is interacting and when it is noninteracting. The effective temperatures for the interacting and noninteracting cases are shown in Figure 8.

First of all, we see in Figure 8 that the overall increase of the fraction of hot particles leads to increase of the effective temperature of the tracer. This is by no means surprising, because the tracer drains energy to the cold particles, but not to the hot ones. A slightly more subtle fact is that the interactions between the hot and cold particles decrease the effective temperature or fluctuations of the tracer. For a small fraction of hot particles, we find that increasing the fraction of hot particles has a relatively weaker effect on the effective temperature for interacting hot and cold particles, as indicated by the smaller slope compared to the noninteracting case. On the other hand, when there is a small fraction of cold particles (near $f_h = 1$), increasing the fraction of cold particles slightly can significantly decrease the effective temperature of the tracer in the interacting case. This is indicated by the steeper slope compared to the noninteracting case.

To make sense of this and subsequent observations, we can resort again to a phenomenological argument similar to formula (6). The simplest and most naive assumption here would be to imagine that the friction experienced by the tracer is the sum of frictions against hot and against cold particles, and similarly that random kicks from hot and cold particles simply add up. This would lead to the expression

$$T_{\rm eff} = \frac{T_h\Gamma + f_h T_h \Gamma_h + f_c T_c \Gamma_c}{\Gamma + f_h \Gamma_h + f_c \Gamma_c}\,, \qquad (7)$$

where $f_c + f_h = 1$. In reality, the additivity of forces behind formula (7) should be approximately valid only for non-interacting particles. Moreover, in that case we additionally assume $\Gamma_h = \Gamma_c$ for noninteracting particles, because the particles in our model are the same in all respects except temperatures. Under this additional assumption, formula (7) predicts a linear dependence of effective temperature on the fraction of hot particles f_h. This prediction is consistent with the data for non-interacting particles (shown in green in Figure 8). This result is qualitatively consistent with the intuition, outlined above in the introduction, that fluctuations should in general be proportional to the power of the driving source, which for noninteracting particles can be thought of as a weighted averaged temperature of particles. An explicit calculation for a warm-up model where particles are connected to the tracer by harmonic springs yields a similar formula (see Appendix equation (11)), but only for particles that do not interact themselves. In fact, even for particles that do not interact to one another directly, formula (7) is not exact, because particles in any case interact indirectly, via exchanges of energy and momentum with the tracer. For directly interacting hot and cold particles, we do not expect this formula to hold as it is too naive. Not surprisingly, Figure 8 definitely shows a non-linear dependence on the hot fraction f_h. The most dramatic deviation from linearity is observed in the range where activity-induced phase separation is most pronounced. In particular, in the vicinity of that range, fluctuations are noticeably below the level predicted by the naive linear theory (7), thus giving at least a hint on how activity can reduce fluctuations.

Since effective temperature $T_{\rm eff}$ of tracer fluctuations is controlled by how much energy is dumped out from the tracer to cold particles, we found it useful to look at how many cold particles are, on average, located within the interaction distance of the tracer. Indeed, the effect of interactions is very noticeable when we look at the number of particles touching the tracer, and in particular the fraction of those that are hot or cold. We refer to this as the local fraction of hot or cold particles, which is different from the global fraction of hot or cold particles in the entire system. These are shown in Figure 9, for two characteristic temperature ratios. When $T_c/T_h = 0.8$, i.e., when the system is not very far from equilibrium, local fractions are hardly different from global ones for both interacting and non-interacting cases. The situation is very different when $T_c/T_h = 0.05$, and strong phase separation becomes possible. In the noninteracting case, the fraction of local cold particles decreases, and turns out significantly smaller than global, meaning that cold particles are being pushed away from the tracer. Our current interpretation of this is that the cold particles diffuse too slowly and are unable to fill any voids created by the moving tracer, similar to the mechanism discussed above in connection with Figure 3. By contrast, in the interacting case, local fraction of cold particles is greater than global, suggesting that cold particles have an increased tendency to stay near the tracer. This recruitment of cold particles to the surface of the tracer could be responsible for dampening its fluctuations. Thus, increasing the activity of the suspension has the effect of keeping cold/passive particles from being pushed away. In the Appendix Figure 15 we present the same data in terms of local numbers (rather than fractions) of local cold and hot particles.

To check the consistency of our results, we analyze the distributions of $\mathbf{R}^2$ for the tracer submerged in the mixture of hot and cold particles, and establish that it remains Gaussian within the accuracy of our simulations, as show in Figure 10 for interacting particles and in the Appendix Figure 14 for non-interacting ones.

5 Discussion and conclusions

In this article, we studied the properties of a suspension of hot/active and cold/passive particles by measuring the fluctuations or effective temperature of a tracer harmonically trapped within the suspension. A simple observation is that the effective temperature of the tracer is essentially a weighted average of the temperatures of the tracer, hot, and cold particles. Thus, the presence of particles with a lower temperature or activity has

the potential to dampen the fluctuations of another more active object. A more subtle and more interesting observation, which is the key result of this work, is made using Brownian dynamics simulations of a tracer in a suspension of hot and cold Brownian particles. We found that interactions between hot and cold particles had a tendency to push cold particles near the tracer. This increases the local fraction of cold particles relative to the global fraction and effectively diminishes the influence of the hot particles. We observed that interactions between hot and cold particles – something that leads to phase separation between active (hot) and passive (cold) particles – may have an especially strong dampening effect on tracer fluctuations, by exposing it to a disproportionally large number of cold particles.

In some way, the activity-driven pacifying of fluctuations can be compared to some mechanical systems, such as, e.g., Kapitza pendulum[35] (see also a textbook presentation[36]), where rapid oscillatory vertical drive of the pivot leads to stabilization of the otherwise unstable "upside-down" position. This analogy, however attractive, is nevertheless rather superficial, because in Kapitza pendulum case what drive does is it modifies the dynamics to make a state stable against fluctuations, while in our case the drive can rather be thought of as suppressing the source of fluctuations.

Another interesting parallel of our results has to do with thermodynamic restrictions on the amount of dissipation associated with measuring information (see, e.g., recent work[37] and references therein).

Although our work was motivated by a certain observations on nuclear dynamics, that nuclear envelope fluctuations could be reduced by the active processes in the nucleoplasm, it is worth emphasizing that our results may be also considered on their own merit, and may potentially find other applications. Our model with the tracer is designed to analyze the possibility of reducing fluctuations by activity, but it should not be viewed as a suggestion to employ our tethered particle as a reporting probe in a microrheology style experiment to examine the far-from-equilibrium properties of an active medium, because it strongly affects and perturbs the medium. This fact can be clearly seen in the simulations snapshots shown in our paper. One easy observation is that our tracer is very frequently found at the interface between hot and cold. One related question that we hope to be able to address in the future would be if the presence of a tracer facilitates the formation of such interface and helps nucleate a new phase out of a uniform mixture. Another view on the same problem would be to frame the issue in terms of wetting. Indeed, pacifying the fluctuations in our model, of course, occurs when (and because) the tracer comes in contact with cold particles, and therefore, the effect will be enhanced if the tracer was well wetted by the cold particles, which can be achieved by introducing, for example, an attractive short range interactions, or thin potential well along the tracer surface for cold particles. In addition, it would be interesting to study if different surfaces, such as the inner surface of a membrane, may have different wetting properties with respect to the cold particles due to the geometry. For example, a concave inner surface of a membrane could potentially have enhanced wetting compared to the convex outer surface of a tracer. It is worth noting, simply as a loose analogy, that an active system of self-propelled or Ornstein-Uhlenbeck particles shows a tendency to have enhanced accumulation on concave surfaces rather than convex ones[38–41].

In this work, we described the fluctuations of the tracer particle in terms of the effective temperature which we determined from the long time mean squared average position of the tracer. One may potentially seek a more detailed description using an approach that would be the direct computational counterpart of the experimental procedure employed in the work on red blood cells[2]. This would require two separate simulations: first, recording a time dependent fluctuation of the tracer position and finding its power spectrum; second, driving the tracer (still surrounded by the same mixture of hot and cold particles) by an external force at various frequencies and measuring the corresponding response function. With these two parts separately determined, one could use the fluctuation-dissipation relation (1a) to define a new effective temperature, $T_{\text{eff}}(\omega)$, which will be frequency-dependent since the system is out of equilibrium.

Returning to the nuclear envelope, we should emphasize that our model is at most a possible scheme as it is in no way a theory of nuclear envelope fluctuations. Nevertheless, we can speculate that maybe the interactions between the more active and less active elements of chromatin and nucleoplasm can lead to the envelope being disproportionally exposed to the less active component. To this end, we can only mention that the segregation between euchromatin and heterochromatin is at least not independent of their different levels of activity[42]. The question that remains to be answered is how much lower can the local activity be. In the case of the nuclear envelope, the motor activity in the genome can lead to fluctuations that are actually smaller than thermal fluctuations, observed in absence of cytoskeletal activity[5]. This peculiar phenomenology occurs due to presence of active systems, the genome and cytoskeleton, on either side of the nuclear envelope. The combined active processes enable fluctuations, which can be both lower or higher than the thermal fluctuations, which may be of critical importance for cellular processes such as the nuclear transport or gene regulation. Obviously, we may even need to consider a different system geometry such as a membrane surrounded by hot and cold particles, which will require further simulations. But the most tantalizing general question is whether one could come up with some general thermodynamic bound on the possible level to which activity can dampen fluctuations.

Conflicts of interest

There are no conflicts to declare.

Acknowledgements

We would like to thank P. Chaikin for useful discussions. AZ was supported in part by the NSF MRSEC Program Grant DMR-1420073 and NSF CAREER Grant PHY-1554880. AYG's research is supported in part by the MRSEC Program of the National Science Foundation under Award DMR-1420073. AYG acknowledges the Aspen Center for Physics where part of this work was written with the support of the National Science Foundation grant number PHY-1607611.

Notes and references

1 L. D. Landau and E. M. Lifshitz, *Statistical Physics, Part 1 (Course of Theoretical Physics, Volume 5)*, Butterworth-Heinemann; 3 edition, 1980, p. 544.

2 H. Turlier, D. Fedosov, B. Audoly, T. Auth, N. Gov, C. Sykes, J.-F. Joanny, G. Gompper and T. Betz, *Nature Physics*, 2016, **12**, 513 – 519.

3 A. Zidovska, D. A. Weitz and T. J. Mitchison, *Proc. Natl. Ac. Sci. USA*, 2013, **110**, 15555–15560.

4 R. Bruinsma, A. Y. Grosberg, Y. Rabin and A. Zidovska, *Biophysical Journal*, 2014, **106**, 1871 – 1881.

5 F.-Y. Chu, S. C. Haley and A. Zidovska, *Proc. Natl. Ac. Sci. USA*, 2017, **114**, 10338–10343.

6 A. Németh and G. Längst, *Trends in Genetics*, 2011, **27**, 149 – 156.

7 K. L. Jost, B. Bertulat and M. C. Cardoso, *Chromosoma*, 2012, **121**, 555 – 563.

8 B. D. Towbin, A. Gonzales-Sandoval and S. M. Gasser, *Trends in Biochem. Sci.*, 2013, **38**, 356 – 363.

9 J. Padeken and P. Heun, *Current Opinion in Cell Biology*, 2014, **28**, 54 – 60.

10 C. M. Caragine, S. C. Haley and A. Zidovska, *eLife*, 2019, **8**, e47533.

11 J. Stenhammar, R. Wittkowski, D. Marenduzzo and M. E. Cates, *Phys. Rev. Lett.*, 2015, **114**, 018301.

12 S. N. Weber, C. A. Weber and E. Frey, *Phys. Rev. Lett.*, 2016, **116**, 058301.

13 J. Smrek and K. Kremer, *Phys. Rev. Lett.*, 2017, **118**, 098002.

14 J. Smrek and K. Kremer, *Entropy*, 2018, **20**, 520.

15 P. Dolai, A. Simha and S. Mishra, *Soft Matter*, 2018, **14**, 6137.

16 R. Exartier and L. Peliti, *Phys. Lett. A*, 1999, **261**, 94 – 97.

17 D. Rings, R. Schachoff, M. Selmke, F. Cichos and K. Kroy, *Phys. Rev. Lett.*, 2010, **105**, 090604.

18 A. Crisanti, A. Puglisi and D. Villamaina, *Phys. Rev. E*, 2012, **85**, 061127.

19 V. Dotsenko, A. Maciolek, O. Vasilyev and G. Oshanin, *Phys. Rev. E*, 2013, **87**, 062130.

20 G. Szamel, *Phys. Rev. E*, 2014, **90**, 012111.

21 G. Falasco, M. V. Gnann, D. Rings and K. Kroy, *Phys. Rev. E*, 2014, **90**, 032131.

22 A. Y. Grosberg and J.-F. Joanny, *Phys. Rev. E*, 2015, **92**, 032118.

23 G. Falasco, M. Baiesi, L. Molinaro, L. Conti and G. Baldovin, *Phys. Rev. E*, 2015, **92**, 022129.

24 H. Tanaka, A. A. Lee and M. P. Brenner, *Phys. Rev. Fluids*, 2017, **2**, 043103.

25 H. C. Fogedby and A. Imparato, *EuroPhysics Lett.*, 2017, **119**, 50007.

26 F. Mura, G. Gradziuk and C. P. Broedersz, *Phys. Rev. Lett.*, 2018, **121**, 038002.

27 A. Y. Grosberg and J.-F. Joanny, *Polymer Science, Series C*, 2018, **60**, 118 – 121.

28 R. R. Netz, *J. Chem. Phys.*, 2018, **148**, 185101.

29 E. Ilker and J.-F. Joanny, *Phys. Rev. Research*, 2020, **2**, 023200.

30 M. Wang and A. Y. Grosberg, *Phys. Rev. E*, 2020, **101**, 032131.

31 E. Ilker, M. Castellana and J.-F. Joanny, *Phys. Rev. Research*, 2021, **3**, 023207.

32 A. Einstein, *Annalen der Physik*, 1906, **324**, 289 – 306.

33 E. W. J. Mardles, *Nature*, 1940, **145**, 970 – 970.

34 B. M. Guy, M. Hermes and W. C. K. Poon, *Phys. Rev. Lett.*, 2015, **115**, 088304.

35 P. Kapitza, *Soviet Phys. JETP*, 1951, **21**, 588 – 597.

36 L. D. Landau and E. M. Lifshitz, *Mechanics (Course of Theoretical Physics, Volume 1)*, Butterworth-Heinemann; 3 edition, 1976, p. 291.

37 M. Rico-Pasto, R. K. Schmitt, M. Ribezzi-Crivellari, J. M. R. Parrondo, H. Linke, J. Johansson and F. Ritort, *Phys. Rev. X*, 2021, **11**, 031052.

38 N. Nikola, A. P. Solon, Y. Kafri, M. Kardar, J. Tailleur and R. Voituriez, *Phys. Rev. Lett.*, 2016, **117**, 098001.

39 C. Sandford, A. Y. Grosberg and J.-F. Joanny, *Phys. Rev. E*, 2017, **96**, 052605.

40 A. Duzgan and J. V. Sellinger, *Phys. Rev. E*, 2018, **97**, 032606.

41 C. Sandford and A. Y. Grosberg, *Phys. Rev. E*, 2018, **97**, 012602.

42 N. Ganai, S. Sengupta and G. I. Menon, *Nucleic Acids Research*, 2014, **42**, 4145–4159.

43 J. D. Weeks, D. Chandler and H. C. Andersen, *J. Chem. Phys.*, 1971, **54**, 5237 – 5247.

44 R. Kubo, *J Phys. Soc. Japan*, 1957, **12**, 570 – 586.

A Additional figures

Figures 12, 13, 14, and 15 are referred to and explained in the main text.

B Simulation details

B.1 Setup

As mentioned, we perform Brownian dynamics simulations using the Langevin equations given by Eqs. (2a), (2b), and (2c). The Langevin equations are integrated using a basic Euler-Maruyama scheme. Unless otherwise mentioned, we assume that $T_{\rm tr} = T_{\rm h} = 1$ and $T_{\rm c} = 0.05$, which corresponds to $T_{\rm h}/T_{\rm c} = 20$. We choose the temperature of the tracer to be the same as the hot particles so that it is "active", much like how a nuclear membrane is active due to nuclear pores and the surrounding cell. All the particles interact through a Weeks-Chandler-Andersen (WCA) potential[43] given by

$$U(r) = \begin{cases} 4\varepsilon\left[\left(\frac{\sigma_{ij}}{r}\right)^{12} - \left(\frac{\sigma_{ij}}{r}\right)^{6}\right] + \varepsilon, & r \le 2^{1/6}\sigma_{ij} \\ 0, & r \ge 2^{1/6}\sigma_{ij} \end{cases} \tag{8}$$

where $\sigma_{ij} = (\sigma_i + \sigma_j)/2$, which is the average of the diameters of the interacting pair i, j. We set $\varepsilon = 50$ so that the hot and cold particles see essentially the same sized tracer. We set the diameter of the tracer to $\sigma_{\rm tr} = 20$ and the diameter of the hot and cold particles to $\sigma_{\rm h} = \sigma_{\rm c} = 2$. The friction coefficients are then set at $\Gamma = 20$ and $\gamma = 2$ to reflect these sizes. The stiffness

of the spring that tethers the tracer is $K = 0.1$. The simulation region has dimensions 150×150 and is periodic in both directions. Unless otherwise stated, the Brownian particles fill the simulation region with a packing fraction of roughly $\phi = 0.4$. The timestep is $dt = 0.0005$ and each simulation is run for 10^9 steps. For each set of parameters, we perform several independent runs and average the results.

To obtain the $\langle \mathbf{R}^2 \rangle$, we simply average multiple realizations of $R^2(t)$. Figure 2 shows the trajectory for $f_h = 0$ and $f_h = 1$. When the tracer is by itself in a viscous solvent, we should expect

$$\left\langle \mathbf{R}^2 \right\rangle (t) = \frac{2T_h}{K}\left(1 - e^{-\frac{K}{\Gamma}t}\right). \tag{9}$$

For our choice of spring constant and friction coefficient, the relaxation time of the tracer should be of order $\tau \sim \Gamma/K$, corresponding to roughly $10^5 - 10^6$ steps, which is much shorter than the timescales we are looking at. Thus the system has equilibrated. As we see for the case of f_h, $\langle \mathbf{R}^2 \rangle (t)$ fluctuates about $2T_h/K$, which is expected from the equipartition theorem. We obtain $\langle \mathbf{R}^2 \rangle$ by averaging the last 90% of the data. Finally, the effective temperature T_{eff} is obtained from the relation $\langle \mathbf{R}^2 \rangle = \frac{d}{K} T_{\text{eff}}$.

C Simple example: particles connected to the tracer via quadratic interactions

To get a better feel for how a tethered tracer might behave in a mixture of hot and cold Brownian particles, we here consider the exactly solvable case when the particles in the mixture interact with the tracer through a pairwise quadratic potential. In other words, the tracer is tethered to the origin and the particles in the mixture are tethered to the tracer with spring constants K and k, respectively. A schematic is shown in Figure 11. Suppose there are N_h hot particles, N_c cold particles, and a tracer driven by thermostats with temperatures T_h, T_c, and T_{tr}, respectively. Let $\mathbf{R}$ and $\mathbf{r}_{h,i}, \mathbf{r}_{c,i}$ denote the positions of the bead and hot/cold particles in the mixture, respectively. The Langevin equations for this system are given by

$$\Gamma \dot{\mathbf{R}} = -K\mathbf{R} - \sum_{i=1}^{N_h} k(\mathbf{R} - \mathbf{r}_{h,i}) - \sum_{i=1}^{N_c} k(\mathbf{R} - \mathbf{r}_{c,i}) + \sqrt{2k_B T_{tr}\Gamma}\xi_{tr}, \tag{10a}$$

$$\gamma \dot{\mathbf{r}}_{h,i} = -k(\mathbf{r}_{h,i} - \mathbf{R}) + \sqrt{2k_B T_h \gamma}\xi_{h,i}, \tag{10b}$$

$$\gamma \dot{\mathbf{r}}_{c,i} = -k(\mathbf{r}_{c,i} - \mathbf{R}) + \sqrt{2k_B T_c \gamma}\xi_{c,i}, \tag{10c}$$

where Γ and γ are the friction coefficients of the bead and hot/cold particles, respectively. ξ_{tr}, $\xi_{h,i}$, and $\xi_{c,i}$ are independent zero-mean, unit-variance Gaussian white noises. There are numerous ways of determining $\langle \mathbf{R}^2 \rangle$. The main result is that the effective temperature takes on the form of the weighted average

$$\begin{aligned} T_{\text{eff}} = \frac{K\langle \mathbf{R}^2 \rangle}{d} &= \frac{k\Gamma + K\gamma}{k\Gamma + K\gamma + Nk\gamma} T_{tr} \\ &+ \frac{N_h k\gamma}{k\Gamma + K\gamma + Nk\gamma} T_h \\ &+ \frac{N_c k\gamma}{k\Gamma + K\gamma + Nk\gamma} T_c, \end{aligned} \tag{11}$$

where $N = N_h + N_c$ is the total number of particles.

For our present purposes, let us assume that the tracer has the same temperature or activity as the hot particles, that is, $T_{tr} = T_h$. There are two extremes. When there are no cold particles ($N_c = 0$), the system is in equilibrium and we get $T_{\text{eff}} = T_h$ or $\langle \mathbf{R}^2 \rangle = dT_h/K$ as expected from the equipartition theorem. On the other hand, when there are no hot particles ($N_h = 0$), the effective temperature of the tracer is brought down to a lower temperature $T_c < T_{\text{eff}}|_{N_h=0} < T_h$. Assuming that N is fixed, a mixture of hot and cold particles will bring the tracer to an intermediate temperature $T_{\text{eff}}|_{N_h=0} < T_{\text{eff}} < T_h$. This is clearer if we take N to be large such that $Nk\gamma \gg k\Gamma + K\gamma$, then the effective temperature becomes the simple average

$$T_{\text{eff}}|_{N \text{ large}} = \frac{N_h T_h + N_c T_c}{N_h + N_c}. \tag{12}$$

It is worth looking at the effective dynamics of the tracer when the rest of the particles are integrated out. Eliminating $\mathbf{r}_{h,i}$ and $\mathbf{r}_{c,i}$ from the Langevin equations, we obtain

$$\int_{-\infty}^{t} \Gamma_{\text{eff}}(t-\tau)\dot{\mathbf{R}}(\tau)d\tau = -K\mathbf{R} + \Xi_{\text{eff}}, \tag{13}$$

where the effective friction kernel Γ_{eff} and effective noise Ξ_{eff} are

$$\Gamma_{\text{eff}}(t-\tau) = \begin{cases} \Gamma\delta_o(t-\tau) + Nke^{-\frac{k}{\gamma}(t-\tau)}, & t-\tau > 0 \\ 0, & t-\tau < 0 \end{cases} \tag{14a}$$

$$\begin{aligned} \Xi_{\text{eff}}(t) = &\sqrt{2k_B T_{tr}\Gamma}\xi_{tr}(t) \\ &+ \sum_{i=1}^{N_h} \frac{k}{\gamma}\sqrt{2k_B T_h \gamma}\int_{-\infty}^{t} e^{-\frac{k}{\gamma}(t-\tau)}\xi_{h,i}(\tau) \\ &+ \sum_{i=1}^{N_c} \frac{k}{\gamma}\sqrt{2k_B T_c \gamma}\int_{-\infty}^{t} e^{-\frac{k}{\gamma}(t-\tau)}\xi_{c,i}(\tau), \end{aligned} \tag{14b}$$

Here, $\delta_o(t-\tau)$ denotes a one-sided delta function, which is required for causality. The noise has correlation

$$\left\langle \Xi_{\text{eff},\alpha}(t)\Xi_{\text{eff},\beta}(t') \right\rangle = 2\delta_{\alpha\beta}k_B T_{tr}\left[\Gamma\delta(t-t') + \frac{(T_h N_h + T_c N_c)k}{2T_{tr}} e^{-\frac{k}{\gamma}|t-t'|}\right]. \tag{15}$$

Note that when $T_h = T_c = T_{tr}$, we have $\left\langle \xi_{\text{eff},\alpha}(t)\xi_{\text{eff},\beta}(t') \right\rangle = \delta_{\alpha\beta}k_B T_{tr}[\Gamma(t-t') + \Gamma(t'-t)]$, which means that fluctuation-dissipation is satisfied and the system should be equilibrium[44].

If we assume that the relaxation time for the interaction between the hot and cold particles and the tracer is much shorter than the relaxation time of the tethered tracer itself or

$$\frac{\gamma}{k} \ll \frac{\Gamma}{K}, \tag{16}$$

which may be true for short-range interactions, we obtain approximately

$$(\Gamma + N\gamma)\dot{\mathbf{R}} = -K\mathbf{R} + \sqrt{2(T_{tr}\Gamma + N_h T_h \gamma + N_c T_c \gamma)}\Xi, \tag{17}$$

where Ξ is a zero mean Gaussian white noise with $\left\langle \Xi_\alpha(t)\Xi_\beta(t') \right\rangle =$

$\delta_{\alpha\beta}\delta(t-t')$. Thus, under the condition Eq. (16) the tracer behaves as though it has an effectively larger friction $\Gamma+N\gamma$ due to the surrounding hot and cold particles and is driven at an effective temperature

$$T_{\rm eff}=\frac{T_{\rm tr}\Gamma+N_{\rm h}T_{\rm h}\gamma+N_{\rm c}T_{\rm c}\gamma}{\Gamma+N\gamma}. \tag{18}$$

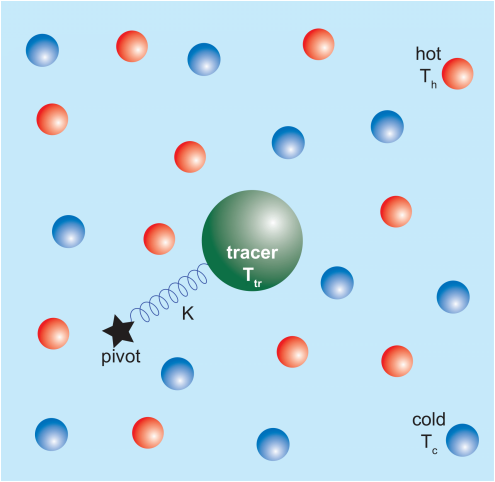

Fig. 1 The tracer is connected to an immobile pivot by a harmonic spring with spring constant K. It is surrounded by a mixture of two types of Brownian particles with different diffusivities or equivalently, with different temperatures $T_{\rm h}$ and $T_{\rm c}$; for brevity, we call these particles hot and cold, respectively. There are $N_{\rm h}$ hot particles and $N_{\rm c}$ cold particles. The tracer itself is connected to yet another thermostat at temperature $T_{\rm tr}$; in most cases below, we assume $T_{\rm tr} = T_{\rm h}$. We examine how the tracer fluctuates around the pivot driven by interactions with particles.

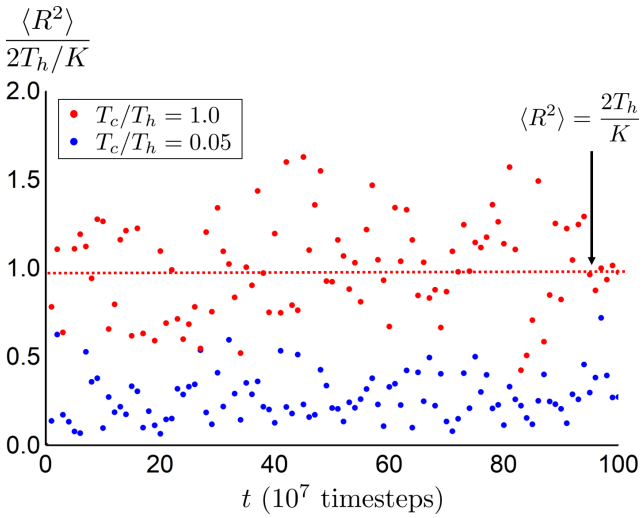

Fig. 2 Plot of the mean-squared displacement of the tracer in contact with a thermostat at temperature T_h surrounded by an interacting bath of Brownian particles with packing fraction $\phi \approx 0.4$ all in contact with a thermostat at temperature T_c for two temperature ratios $T_\mathrm{c}/T_\mathrm{h} = 0.05$ (blue) and $T_\mathrm{c}/T_\mathrm{h} = 1.0$ (red). Each point for $T_\mathrm{c}/T_\mathrm{h}$ = 0.05 (blue) and $T_\mathrm{c}/T_\mathrm{h}$ = 1.0 (red) is averaged over 5 and 10 independent runs, respectively.

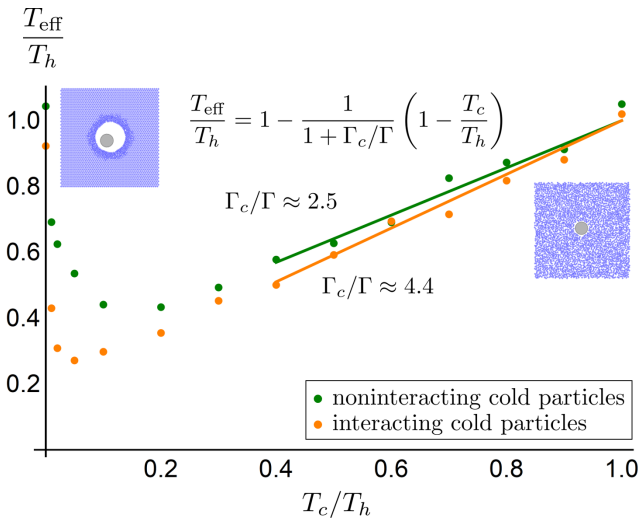

Fig. 3 Plot of the effective temperature of the tracer $T_{\rm eff}$ as a function of the temperature $T_{\rm c}$ of the surrounding bath of cold Brownian particles, which is at packing fraction $\phi = 0.4$. When $T_{\rm c}$ is only moderately below $T_{\rm h}$, the effective temperature is approximately linear which we explain in Eqs. (5) in terms of the friction coefficient of the tracer against solvent Γ and the effective friction coefficient $\Gamma_{\rm c}$ against the cold particles, the latter having different values for interacting and non-interacting cold particles. The insets show that for $T_{\rm c}/T_{\rm h} \ll 1$, the tracer pushes the cold particles away and a void forms around the tracer. As a result, the tracer has more room to diffuse without interacting with the cold particles. This is responsible for the nonmonotonic behavior of $T_{\rm eff}$ for temperatures less than $T_{\rm c}/T_{\rm h} \sim 0.1$.

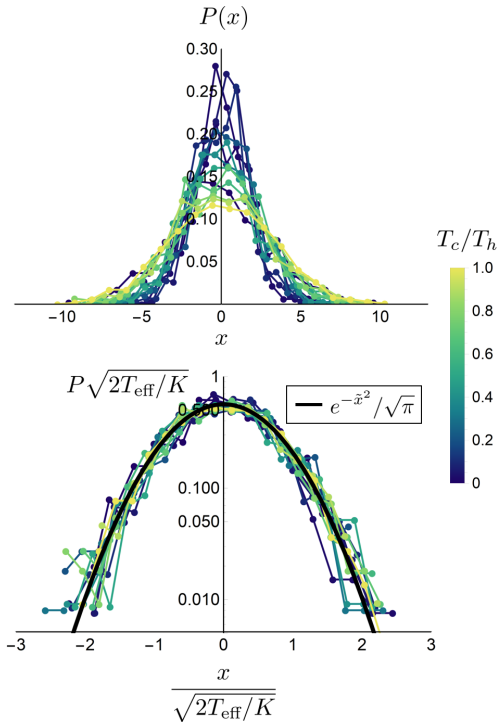

Fig. 4 Plot of the distribution of the x positions of the tracer as a function of the temperature $T_{\rm c}$ of the surrounding cold particles (interacting) with a packing fraction $\phi \approx 0.4$. Rescaling the distributions and positions using the effective temperature $T_{\rm eff}$ obtained from $T_{\rm eff}$ vs $T_{\rm c}$ figure 3, we find that all of the distributions collapse to a single Gaussian distribution.

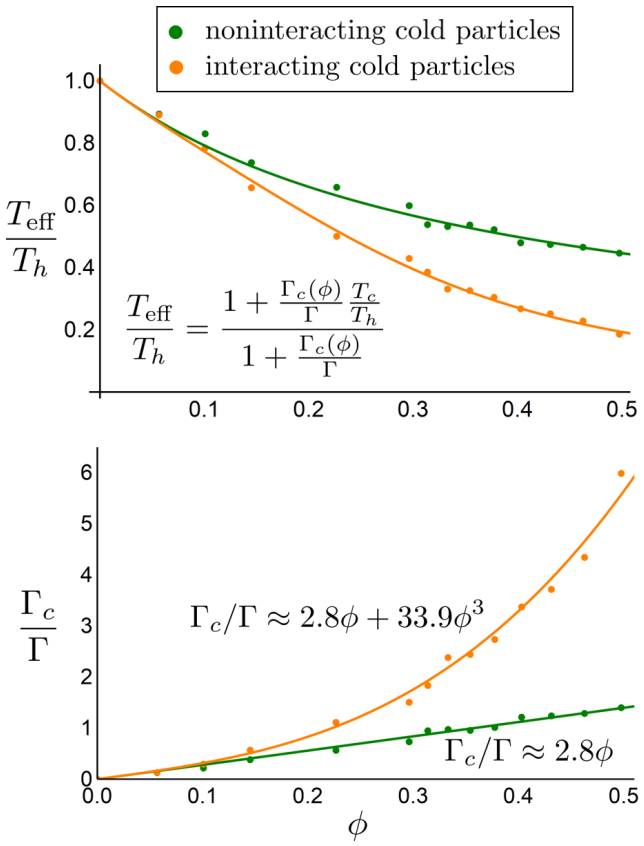

Fig. 5 Upper: Plot of the effective temperature $T_{\rm eff}$ of the tracer as a function of the packing fraction of the surrounding cold Brownian particles. The temperature ratio of the cold particles to the tracer is set to $T_{\rm c}/T_{\rm h} = 0.05$. Interacting cold particles (orange) lower the effective temperature of the tracer more efficiently than when they are noninteracting (green). **Lower:** Plot of the friction $\Gamma_{\rm c}$ due to the surrounding cold particles. The values for $\Gamma_{\rm c}(\phi)$ were obtained by solving equation for $\Gamma_{\rm c}(\phi)$ in terms of $T_{\rm eff}(\phi)$. Fitting $\Gamma_{\rm c}$, we obtained a linear dependence $\Gamma_{\rm c}/\Gamma \approx 2.8\phi$ for noninteracting cold particles (green) and an extra cubic dependence $\Gamma_{\rm c}/\Gamma \approx 2.8\phi + 33.9\phi^3$ for interacting cold particles (orange).

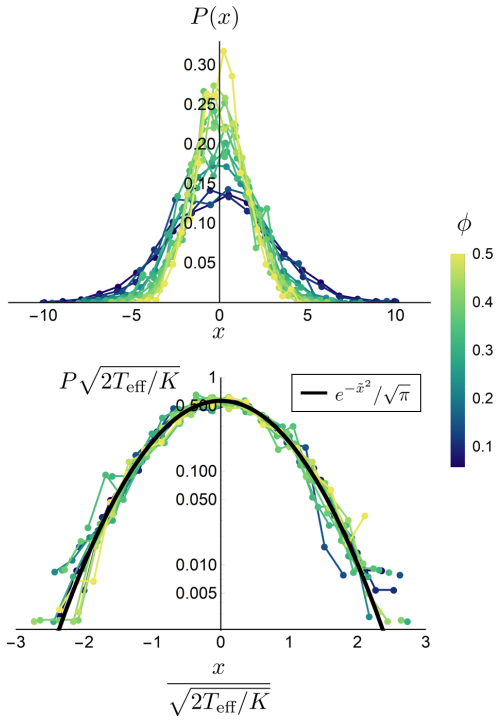

Fig. 6 Plot of the distribution of the x positions of the tracer as a function of the packing fraction ϕ of the surrounding cold particles (interacting) with a temperature ratio $T_{\rm c}/T_{\rm h} = 0.05$. Rescaling the distributions and positions using the effective temperature $T_{\rm eff}$ obtained from $T_{\rm eff}$ vs ϕ figure 5, we find that all of the distributions collapse to a single Gaussian distribution.

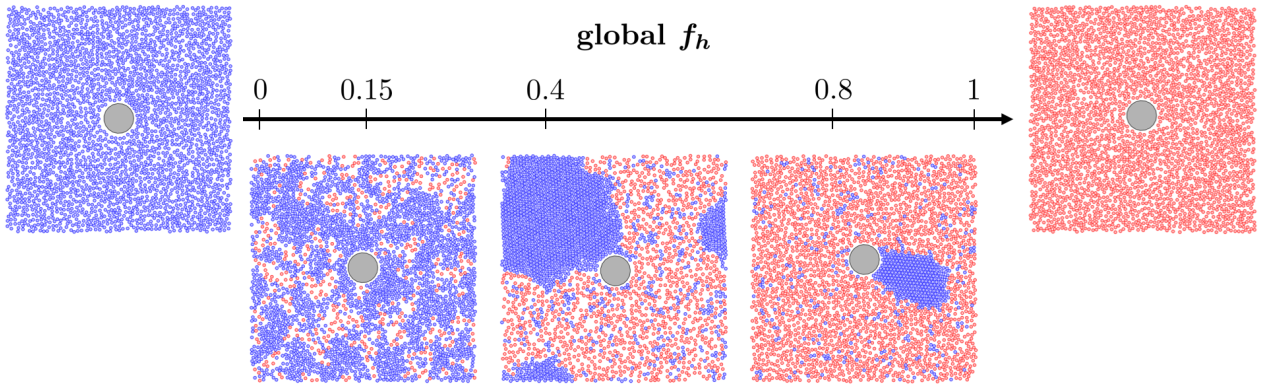

Fig. 7 Snapshots of the simulations for different fractions of hot and cold particles. The global fraction $f_{\rm h}$ is defined as $f_{\rm h} = N_{\rm h}/(N_{\rm h}+N_{\rm c})$ where $N_{\rm h}$ and $N_{\rm c}$ are the total numbers of cold and hot particles in the system. The temperature ratio used in these simulations is $T_{\rm c}/T_{\rm h} = 0.05$.

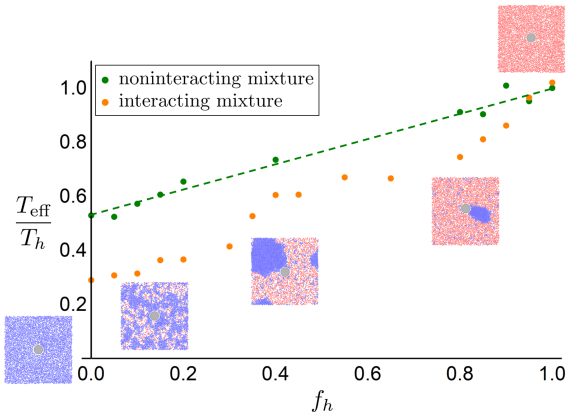

Fig. 8 Plot of the effective temperature $T_{\rm eff}$ of the tracer as a function of the global fraction $f_{\rm h}$ of interacting (orange) or noninteracting (green) hot and cold Brownian particles in the system. The dashed green line indicates a linear dependence on $f_{\rm h}$ as expected from Eq. (7) under the assumption $\Gamma_{\rm h} = \Gamma_{\rm c}$. There is a hump in $T_{\rm eff}$ for an interacting bath over the range $0.3 < f_{\rm h} < 0.7$. Over this range, there is a strong phase separation and it can be seen that the tracer tends to be located near the surface of the cluster of cold particles, allowing it to also contact many hot particles.

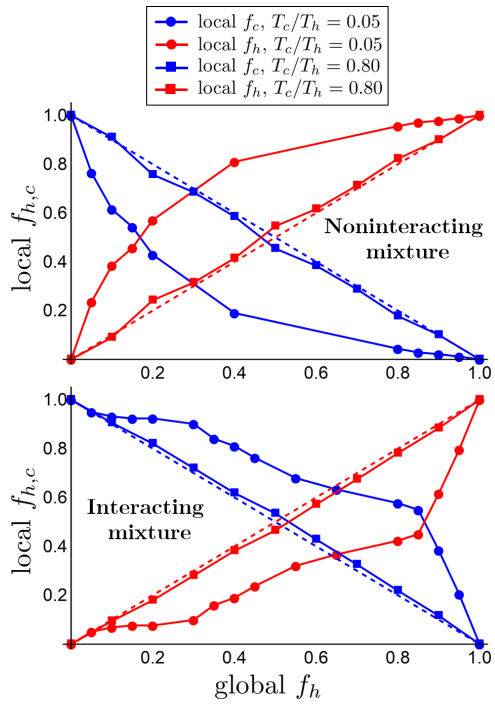

Fig. 9 Plot of the local fractions of hot and cold particles as a function of the global fractions for temperature ratios $T_c/T_h = 0.05, 0.8$. "Local" particles are defined as those within a Lennard-Jones cutoff distance $r < 2^{1/6}(a_{tr} + a)$ of the tracer, where a_{tr} and a are the radii of the tracer and bath particles, respectively. We average over many frames to determine the average numbers of cold and hot particles interacting with the tracer in order to determine the local fractions. The packing fraction of hot and cold particles is $\phi \approx 0.4$. For a noninteracting mixture (left), there is a tendency for the cold particles to be pushed away by the tracer. For an interacting mixture (right), however, the interactions between the hot and cold particles tends to keep cold particles near the tracer, leading to more interactions with the cold particles.

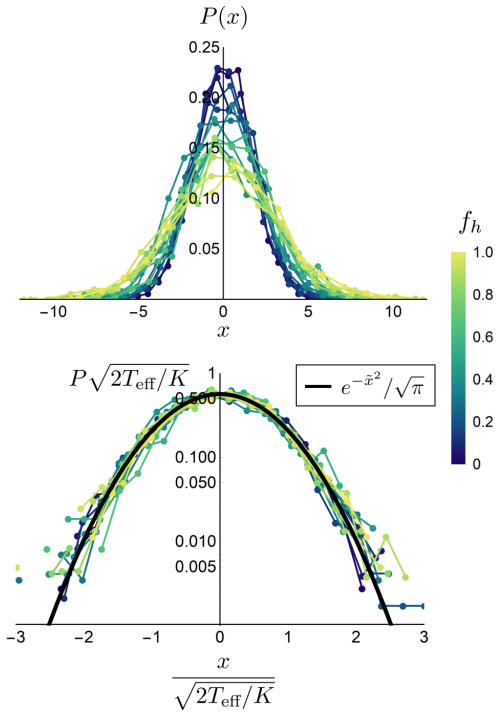

Fig. 10 Plot of the distributions of the x positions of the tracer as a function of the global fraction $f_{\rm h}$ of interacting hot and cold particles. The temperature ratio is $T_{\rm c}/T_{\rm h} = 0.05$ and the packing fraction is $\phi \approx 0.4$. Rescaling the distributions and positions using the effective temperature $T_{\rm eff}$ obtained from $T_{\rm eff}$ vs $f_{\rm h}$ figure 8, we find that all of the distributions collapse onto a Gaussian distribution.

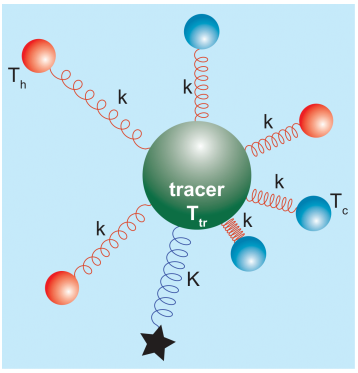

Fig. 11 Schematic for the warm-up example in Section C, when the tracer interacts with the hot and cold particles through pairwise quadratic potentials or ideal springs.

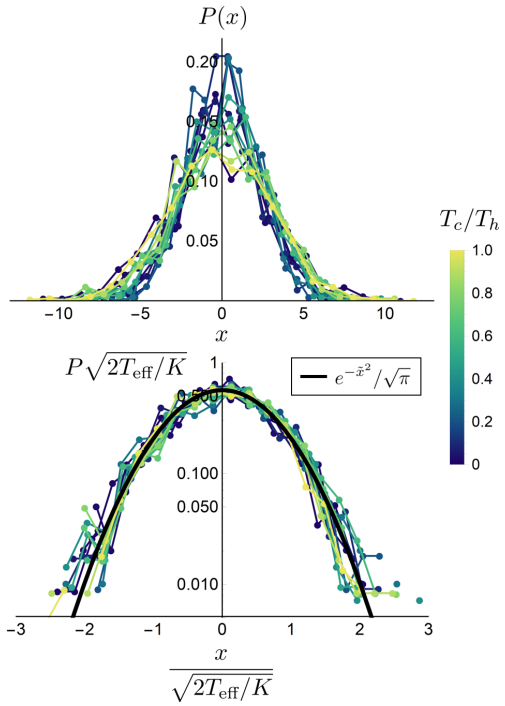

Fig. 12 Plot of the distribution of the x positions of the tracer as a function of the temperature $T_{\rm c}$ of the surrounding cold particles (noninteracting) with a packing fraction $\phi \approx 0.4$. Rescaling the distributions and positions using the effective temperature $T_{\rm eff}$ obtained from [$T_{\rm eff}$ vs $T_{\rm c}$ figure], we find that all of the distributions collapse to a single Gaussian distribution.

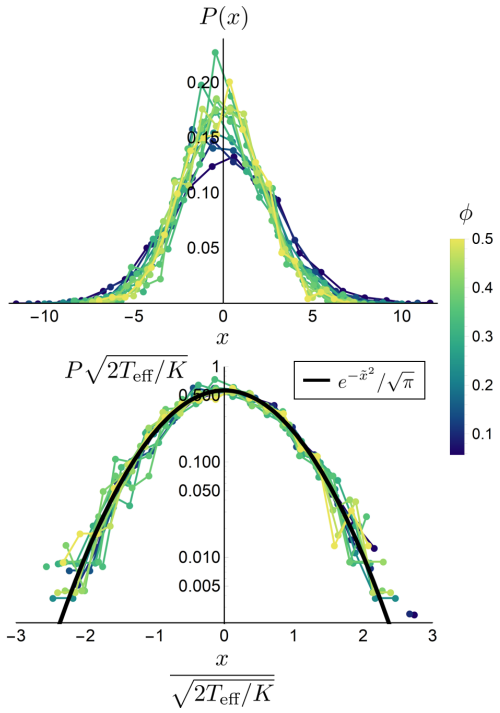

Fig. 13 Plot of the distribution of the x positions of the tracer as a function of the packing fraction ϕ of the surrounding cold particles (noninteracting) with a temperature ratio $T_{\rm c}/T_{\rm h} = 0.05$. Rescaling the distributions and positions using the effective temperature $T_{\rm eff}$ obtained from [$T_{\rm eff}$ vs ϕ figure], we find that all of the distributions collapse to a single Gaussian distribution.

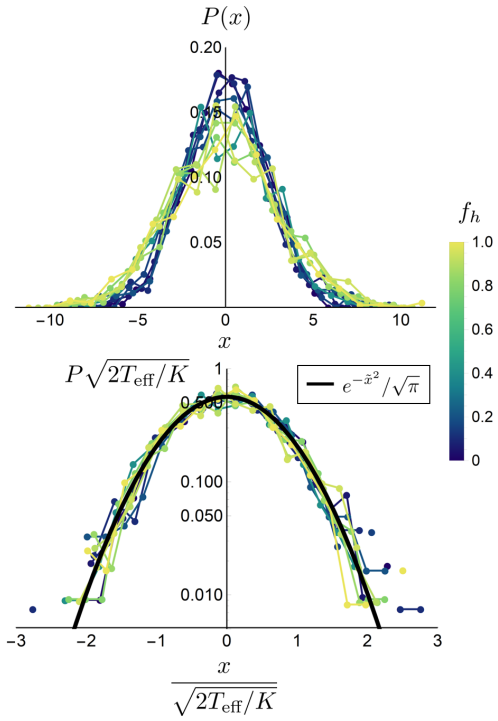

Fig. 14 Plot of the distributions of the x positions of the tracer as a function of the global fraction $f_{\rm h}$ of noninteracting hot and cold particles. The temperature ratio is $T_{\rm c}/T_{\rm h} = 0.05$ and the packing fraction is $\phi \approx 0.4$. Rescaling the distributions and positions using the effective temperature $T_{\rm eff}$ obtained from [$T_{\rm eff}$ vs $f_{\rm h}$ figure], we find that all of the distributions collapse onto a single Gaussian distribution.

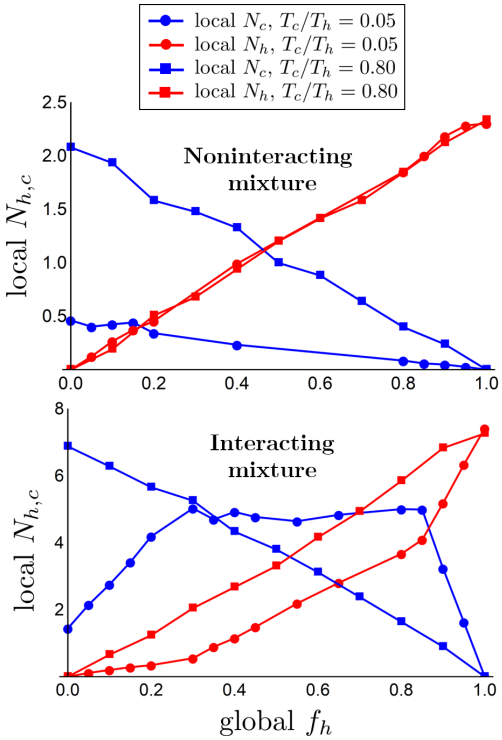

Fig. 15 Plot of the local numbers of hot and cold particles interacting with the tracer. "Local" means particles that are with the Lennard-Jones cutoff distance of the tracer ($r < 2^{1/6}(a_{\rm tr} + a)$). For a noninterating mixture (left), increasing the global fraction of hot particles simple decreases the local number of cold particles linearly. For an interacting mixture (right), however, increasing the global fraction of hot particles actually increases the local number of cold particles over the range $f_{\rm h} < 0.3$, suggesting the the hot particles tend to push the cold particles to the surface of the tracer.